





Article

Experimental Investigation and NSGA-III Multi-Criteria Optimization of 60CrMoV18-5 Cold-Work Tool Steel Machinability Under Dry CNC Hard Turning Conditions

Nikolaos A. Fountas ^{1,*}, Ioannis G. Papantoniou ², Dimitrios E. Manolakos ² and Nikolaos M. Vaxevanidis ^{1,*}

¹ Laboratory of Manufacturing Processes and Machine Tools (LMProMaT), Department of Mechanical Engineering Educators, School of Pedagogical and Technological Education (ASPETE), GR 151 22 Amarousion, Greece

² School of Mechanical Engineering, National Technical University of Athens, GR 157 80 Zografou, Greece; ipapanto@central.ntua.gr (I.G.P.); manolako@central.ntua.gr (D.E.M.)

* Correspondence: nfountas@aspete.gr (N.A.F.); vaxev@aspete.gr (N.M.V.)

Abstract: This work concerns an experimental investigation dealing with the machinability of 60CrMoV18-5 cold-work tool steel under dry CNC hard turning conditions using a CBN cutting insert. A response surface experiment based on the central composite design was set to conduct dry CNC hard-turning experiments with three different levels for cutting conditions, cutting speed V_c (m/min), feed rate f (mm/rev), and depth of cut a (mm) while selecting main cutting force and surface roughness R_a as the two machinability responses. The results were analyzed by applying analysis of variance (ANOVA). The effect of cutting conditions on main cutting force and surface roughness was studied through contour plots. Full quadratic regression models were generated to model the relationships between inputs and outputs. Finally, the NSGA-III algorithm was applied to simultaneously optimize the selected machinability parameters by providing beneficial values for determining cutting conditions. The results have shown that surface roughness is mainly affected by feed rate and cutting speed, whereas main cutting force is affected by depth of cut and feed rate.

Keywords: 60CrMoV18-5 tool steel; CNC turning; machinability; optimization; NSGA-III



Citation: Fountas, N.A.; Papantoniou, I.G.; Manolakos, D.E.; Vaxevanidis, N.M. Experimental Investigation and NSGA-III Multi-Criteria Optimization of 60CrMoV18-5 Cold-Work Tool Steel Machinability Under Dry CNC Hard Turning Conditions. *Machines* **2024**, *12*, 772. <https://doi.org/10.3390/machines12110772>

Academic Editor: Kazumasa Kawasaki

Received: 8 October 2024

Revised: 26 October 2024

Accepted: 1 November 2024

Published: 3 November 2024



Copyright: © 2024 by the authors. Licensee MDPI, Basel, Switzerland. This article is an open access article distributed under the terms and conditions of the Creative Commons Attribution (CC BY) license (<https://creativecommons.org/licenses/by/4.0/>).

1. Introduction

New developments in industrial applications and customers' requirements for reliable products impose the need for ongoing research concerning the machinability of special engineering alloys. To machine engineering alloys, production lines found in industry implement CNC machine tools adhering to either conventional [1–4] or non-conventional material removal principles [5–8]. As regards conventional material removal machining operations, milling, turning, drilling, and grinding are distinguished, all of which are integrated with CNC resources. Rounded bars of cold-work tool steels are preferred to be machined in CNC turning centers or conventional high-power lathes for hard turning. As a machining operation, hard turning utilizes a single-point tool contact and materials to be hard-turned exhibit increased hardness that exceeds 45 HRC [9–12].

Undoubtedly, extensive know-how currently exists concerning a variety of machinability studies presenting different quality aspects for engineering alloys. Nevertheless, the availability of research results as regards machinability does not encourage their generalization towards the prediction of crucial outputs of other materials or special alloys yet to be exploited. Consequently, machinability studies continue exploring key objectives that characterize engineering alloys and other materials related to industrial applications. Material removal by cutting may exhibit complex interactions among independent process parameters (cutting conditions) owing to the mechanics of metal cutting [9]. During metal removal by cutting, a significant outcome owing to increased cutting force components,

rising temperature, and extensive tool wear is experienced with potential tool breakage [13]. This outcome negatively affects surface finish, dimensional accuracy, roughness indicators, and cutting tool life.

Benlahmidi et al. [14] investigated the influence of cutting conditions, including cutting speed, feed rate, depth of cut, and work piece hardness, on the quality criteria of surface roughness, cutting pressure, and cutting power during hard turning of hardened X38CrMoV5-1 (AISI H11) of 50HRC with CBN7020 cutting inserts. They concluded that surface roughness indicators are primarily affected by feed rate and workpiece hardness, whereas the effect of cutting depth was found to be insignificant. The dominant parameter concerning the response of cutting power was cutting speed. The later parameter affects tool life, with feed rate being the second influential parameter in hierarchy as regards tool life response. In [15], Çydaş studied the performance of AISI 4340 steel under dry turning conditions by testing a variety of cutting tools involving CBN, P10-grade carbide and ceramics. The effect of these tools on workpiece hardness was examined as well as surface roughness, tool flank wear, maximum tool-chip interface temperature and micro hardness variations. The results referring to these performance metrics were evaluated by implementing several statistical analysis methods. Santhosh et al. [16] examined the same alloy, AISI 4340, under a systematic design of experiments based on face-centered central composite design (CCD) according to the response surface methodology (RSM). As the independent process parameters, feed rate, rotational speed, and cutting depth were selected, whilst arithmetic surface roughness average was considered as the objective. In addition, the standard genetic algorithm and a neural network topology were applied to suggest an optimal combination among machining parameters and optimize surface roughness response. Abbas et al. [17] conducted an extensive examination on AISI 4340 hard turning using two types of cutting tool geometries: wiper nose and typical round nose tips. Having cutting conditions as the independent variables, they proceeded to simultaneously optimize surface roughness and productivity using MOPSA and MOEPCA algorithms. In their work, MOPSA suggested the optimal solution for parameter setting for the case of wiper cutting inserts, whereas MOEPCA provided the optimal solution for the cutting insert with the conventional rounded tool tip geometry. Chavan and Sargade [18] focused on examining AISI 52100 machinability improvements with coated carbide tools, referring to a group of surface integrity indicators including surface roughness and micro hardness by controlling cutting speed and feed rate under several cutting environments, including dry cutting. Davoudinejada et al. [19] studied the machinability of hardened DF-3 tool steel under continuous dry turning with different cutting conditions. Their objectives under examination were tool life, tool wear, and surface roughness. The cutting insert employed was coated in mixed ceramic with honed edge geometry. They designed their experiments by assigning two levels for cutting speed, three levels for feed rate, and a constant depth of cut equal to 0.2 mm. They found that the lowest cutting speed facilitates tool life as opposed to surface roughness, where reduced results were obtained at high cutting speed and low feed rate. The objective of maximum material volume removal was beneficial when operating with low cutting speed and high feed rate. Flank and crater wear observations were experienced owing to abrasive conditions exerted in the ceramic cutting tool-work piece interface. Sun et al. [20] performed dry cutting experiments on Ti6Al4V alloy using two types of cutting inserts: polycrystalline cubic boron nitride (PCBN) and polycrystalline diamond (PCD). In their work, the influence of cutting speed and feed rate on tool life, cutting temperature, and surface roughness were examined. They reported that chipping, notch, adhesion, and crater were the main failure mechanisms for PCBN cutting insert, whilst adhesion, crater, and dissolution-diffusion were observed in the case of the PCD tool that exhibited better cutting performance. Muthuswamy and Murugesan [21] studied the machinability of Ti6Al4V alloy through a full factorial design of experiments and corresponding analysis of variance. The objectives selected were surface roughness and cutting force components. They mentioned that feed rate is a significant independent variable for Ra , whereas the interactions between feed rate and cutting depth are influential

for cutting forces followed by cutting speed. They used AlTiNPVD-coated tools to conduct their turning experiments. Malik et al. [22] examined the machining behavior of Ti6Al4V alloy by studying different levels of input values for cutting parameters on the responses of cutting force and surface roughness. Interesting results concerning the machinability of laser-melted 316L stainless steel were presented by Li et al. [23]. They examined the effect of cutting depth on cutting force and surface quality, whilst their analysis involved white layer formation at different cutting depths as well as work-hardening and thermal softening mechanisms. Along with the extensive research concerning the machinability attributes for examination and the phenomena that warrant identification with proper analysis, a remarkable amount of research is also directed towards the optimization of crucial performance criteria related either to productivity or quality or both simultaneously. Such criteria are surface roughness parameters, cutting force, cutting temperature, tool wear, tool-chip interface with emphasis to temperature, material removal rate, etc. [24–27]. In addition, several efforts have focused on utilizing the properties of lubricants to study their effect on process-related criteria while they have implemented machine learning techniques for optimization [28–35].

In this framework, the current study focuses on the examination of cutting speed, feed rate and depth of cut effects on cutting forces and surface roughness during dry CNC turning of 60CrMoV18-5 cold-work tool steel. This material is preferred for engineering applications related to injection molds for fabricating plastic components, cold forming tools, cutting blades, stamping equipment, and punches. The variety of applications of 60CrMoV18-5 cold-work tool steel is favored owing to the material's properties such as high toughness and wear resistance. High-stress applications (i.e., cutting tools and special molds) can also be facilitated by the selection of 60CrMoV18-5 cold-work tool steel with working hardness up to 60 HRC.

As an original aspect of this study, the non-dominated sorting genetic algorithm III (NSGA-III) is employed to obtain a variety of non-dominated "optimal" solutions that will balance the trade-off between main cutting force, F_z (N), and surface roughness, R_a (μm), according to the needs and response importance determined by workshops and manufacturing facilities. The methodology for obtaining the number of non-dominated solutions is a pure two-objective optimization problem without its transformation to a single-objective one using weighted coefficients. By taking advantage of the "pre-allocated" function of NSGA-III, referring to the reference set for non-dominated solutions, a stronger diversity is achieved among solutions according to the predetermined population size in the problem domain. The proposed methodology aims at supporting machinability studies for engineering materials towards the major objective of optimizing performance criteria related to general manufacturing processes and machining operations.

2. Materials and Methods

2.1. Design of Experiments

A systematic design of experiments comprising 20 independent tryouts was established with reference to the central composite design (CCD) of Response Surface Methodology (RSM) to examine the effect of cutting conditions: cutting speed V_c , feed rate, and depth of cut on main cutting force, F_z (N), and arithmetic surface roughness average, R_a (μm). This type of experimental design allows for fitting a reliable second-order (full quadratic) regression model by selecting corner, axial, and center points under the assumption that relatively few independent variables are to be questioned [36]. As independent variables, the cutting conditions of cutting speed, V_c (m/min); feed rate, f (mm/rev); and depth of cut, a (mm), were selected whilst varying levels were determined according to the tool vendor's recommendations (Uddeholm®-Swedish). Since the number of independent variables is low enough to reduce experimental cost, the selection of the aforementioned type of experimental design is justified. To maintain an equidistant radial length " r " and therefore a common prediction error magnitude for all experimental points with reference to the center point, the CCD was also rotatable. Given the number of cutting conditions-independent

variables while considering uniform precision, the CCD involves eight factorial, six axial, and six center points, resulting in the total number of 20 runs. Table 1 gives the design of experiments according to the cutting conditions and their levels.

Table 1. Cutting conditions-independent variables and experimental levels.

| Parameter | Symbol | Central Composite Design of Experiments | | | Unit |
|---------------|--------|---|------------|----------|--------|
| | | Level | | | |
| | | Low (−1) | Center (0) | High (1) | |
| Cutting speed | V_c | 141.3 | 164.8 | 188.4 | m/min |
| Feed rate | f | 0.050 | 0.125 | 0.200 | mm/rev |
| Depth of cut | a | 0.500 | 1.000 | 1.500 | mm |

2.2. Materials, Machining Set-Up and Measuring Equipment

Two cylindrical bars of 60CrMoV18-5 cold-work tool steel were used for performing the experiments. The working material was in the form of rounded bars and it was pre-machined to a predetermined reference diameter of $\text{Ø}60$ mm. Based on the material's initial diameter, spindle speed was also computed for CNC programming. To facilitate chip removal among the experimental regions and observe the machining outcome during experimental execution, the available material length was distinguished to 10 regions by formulating grooved cuts among the pre-specified lengths of each rounded bar (Figure 1).

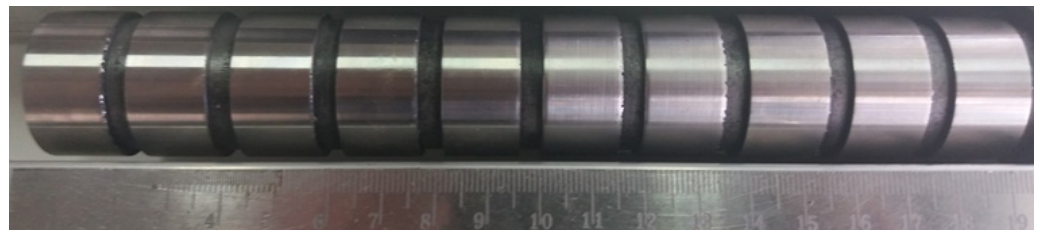


Figure 1. $\text{Ø}30 \times 300$ mm 60CrMoV18-5 cold-work tool steel bar prepared with the 10 discrete experimental zones for dry CNC turning experiments.

The cubic boron nitride (CBN) CBN-200 of SECO with code TNGA332S-00820-L1-C and its corresponding cutting insert holder PTJNR 2525M16 were selected for conducting the CNC dry cutting experiments (Figure 2).

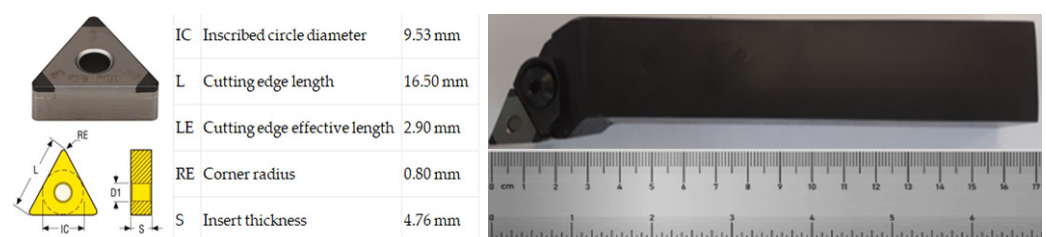


Figure 2. The SECO® TNGA332S-00820-L1-C CBN200 cutting insert mounted to a PTJNR 2525M16 cutting insert holder.

Dry CNC turning experiments were conducted by employing a HAAS® TL-1 CNC turning center (Figure 3a). A Kistler® three-component cutting force dynamometer along with its corresponding data acquisition analog system were used for taking online measurements during turning (Figure 3b).

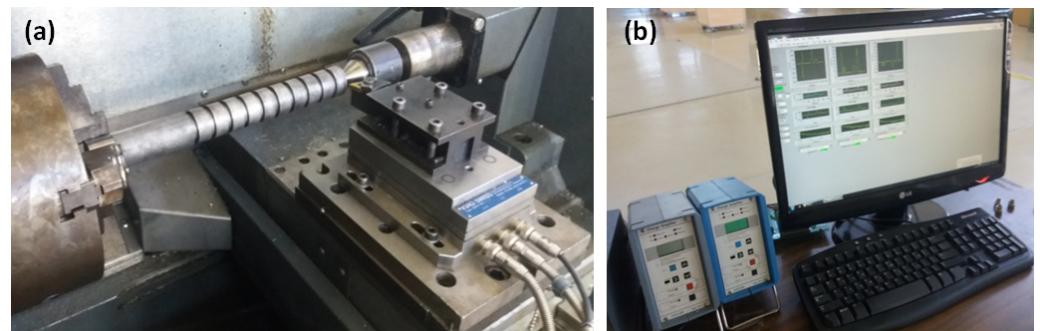


Figure 3. (a) CNC machining set-up for dry CNC turning experiments; (b) Cutting force acquisition/signal processing software environment.

To collect the results regarding surface roughness, the TESA® Rugosurf® 10G portable roughness tester. The set-up for conducting roughness measurements is illustrated in Figure 4. The specific portable roughness tester supports 3 probe measuring positions whilst the measuring span is 400 μm (6300 μin) on Z axis and 16 mm (0.63 in) on X axis, with a probing speed of 1mm/sec. Its display span is 0–100 μm for R_a and 0.05 to 400 μm for R_t whilst its measuring force is 0.75 mN. The graphics supported are Bearing area curve, Profile-R, and Profile-P. A diamond-point 90° stylus is attached to the roughness tester with $R = 5 \mu\text{m}$. The number of cut-off length is 1 to 10 for a cut-off of 0.25 mm and 0.8 mm, whereas the cut-off length may be determined to be equal to 0.25 mm, 0.80 mm, and 2.50 mm (0.01 in-0.03 in-0.10 in). In this work, cut-off length was set to 0.8 mm, whilst measurements were conducted three times for each cutting zone out of three equally positioned generatrices at 120°. As a representative result for roughness, the average value was considered.

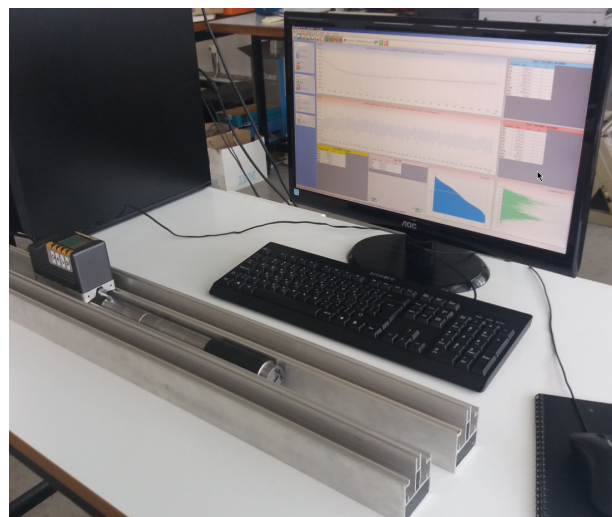


Figure 4. TESA® Rugosurf 10G set-up for roughness measurements.

3. Non-Dominated Sorting Genetic Algorithm, NSGA-III

Intelligent algorithms available in the broader literature exhibit different operational behavior depending on their development attributes and the problem in question. Each algorithm simulates the major physical aspects of living species that are considered search agents. The primary objective of Non-dominated Sorting Genetic Algorithm III (NSGA–III) is to solve optimization cases where many conflicting criteria are to be satisfied. The algorithm suggests enhancements in the preservation of solutions, diversity, and efficiency. This facilitates the consistent approximation of a Pareto front representing the set of non-dominated optimal solutions. NSGA–III adheres to the major aspects of evolutionary optimization. Consequently, NSGA–III employs the standard genetic operators: selection

crossover and mutation with a set of additional functions, namely non-dominated sorting, crowding distance, and environmental selection. Non-dominated sorting classifies individuals (candidate solutions) into different Pareto fronts according to their dominance relationship. Candidates who are not dominated by others formulate the first front in an optimization problem. Candidates that are dominated by those existing on the first front formulate the second front, etc. As a result, non-dominated sorting preserves diversity in a population of candidate solutions. The function responsible for measuring the density of obtained Pareto solutions is crowding distance. Crowding distance maintains well-distributed solutions in a front by controlling the individuals' locations in denser regions referring to the solution domain. The quality and diversity of obtained solutions are controlled by the environmental selection operator in the NSGA-III algorithm. This operator selects candidate solutions from the different fronts regarding their rank and crowding distance, thus allowing a balanced solution representation across the entire front. This procedure sustains diversity and convergence of non-dominated solutions. Other features of the NSGA-III algorithm include reference points, decomposition, and adaptive operator selection. Regardless of the efficiency and operational behavior of the several metaheuristics, algorithm-specific parameters and operators should be fine-tuned and properly determined to maintain a profitable balance between exploration and exploitation of the search domain. The recommended settings for the algorithms examined on the problem under study were adopted by the original attributes provided in [37,38].

4. Results and Discussion

4.1. Experimental Results and Analysis of Observations

The results obtained from conducting the series of experiments as indicated in Table 1 were further processed to avoid the oscillations exhibited owing to arbitrary low and high frequency levels during CNC hard-turning cuts. Original results were processed such that the average values for main cutting force per each cutting region will represent the final output. The experimental results referring to the two objectives of main cutting force, F_z (N), and surface roughness, R_a (μm), according to the design of experiments presented in Table 1, are summarized in Table 2.

Table 2. Experimental results for main cutting force F_z , (N) and surface roughness R_a , (μm).

| No. | V_c (m/min) | f (mm/rev) | a (mm) | F_z (N) | R_a (μm) |
|-----|---------------|--------------|----------|-----------|-------------------------|
| 1 | 141.3 | 0.050 | 0.50 | 128.5 | 1.11 |
| 2 | 188.4 | 0.050 | 0.50 | 104.2 | 0.98 |
| 3 | 141.3 | 0.200 | 0.50 | 208.9 | 4.00 |
| 4 | 188.4 | 0.200 | 0.50 | 179.4 | 3.80 |
| 5 | 141.3 | 0.050 | 1.50 | 181.1 | 1.47 |
| 6 | 188.4 | 0.050 | 1.50 | 157.7 | 1.04 |
| 7 | 141.3 | 0.200 | 1.50 | 381.4 | 4.10 |
| 8 | 188.4 | 0.200 | 1.50 | 370.0 | 3.76 |
| 9 | 164.8 | 0.125 | 1.00 | 241.5 | 2.07 |
| 10 | 164.8 | 0.125 | 1.00 | 236.6 | 1.97 |
| 11 | 164.8 | 0.125 | 1.00 | 346.4 | 1.69 |
| 12 | 164.8 | 0.125 | 1.00 | 327.7 | 1.33 |
| 13 | 126.4 | 0.125 | 1.00 | 331.0 | 1.57 |
| 14 | 203.3 | 0.125 | 1.00 | 285.8 | 1.30 |
| 15 | 164.8 | 0.025 | 1.00 | 83.80 | 0.98 |
| 16 | 164.8 | 0.250 | 1.00 | 404.3 | 8.95 |
| 17 | 164.8 | 0.125 | 0.18 | 22.10 | 1.72 |
| 18 | 164.8 | 0.125 | 1.82 | 266.2 | 1.90 |
| 19 | 164.8 | 0.125 | 1.00 | 236.3 | 1.87 |
| 20 | 164.8 | 0.125 | 1.00 | 241.1 | 1.76 |

It is indicated that the largest magnitude for main cutting force F_z (404.30 N) is observed in the 16th experimental run, where average surface roughness R_a is equal to

8.95 μm . For this experiment, cutting speed V_c is 164.8 m/min (spindle speed, $n = 1750$ rpm), feed rate f is 0.25 mm/rev, and depth of cut α is equal to 1.0 mm. The lowest result for main cutting force F_z is reported in the 17th experiment at 22.10 N. The experiment is accompanied with a resulting surface roughness average R_a equal to 1.72 μm . Figure 5 illustrates the main effects of cutting conditions on main cutting force F_z (N).

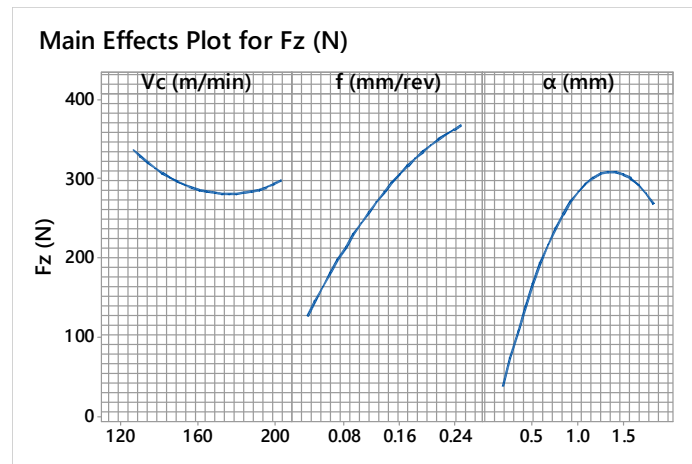


Figure 5. Main effects plot for main cutting force, F_z (N).

According to the observations referring to the main effects of cutting conditions on main cutting force F_z , an increase in cutting speed V_c seems to decrease F_z at least up to a range of moderate settings, i.e., 160–180 m/min. This observation is owing to the machined material's plastic behavior (softening) under the influence of cutting temperature increase. Feed rate f seems to increase main cutting force F_z , but with a small impression of gradual reduction when set to its higher level (i.e., $f = 0.2$ mm/rev) owing to cutting temperature effect and plastic softening. As depth of cut α increases, an increase in main cutting force is also observed, however; high values for depth of cut settings do not necessarily maintain high levels for main cutting force, i.e., $\alpha = 2$ mm. However, the settings of cutting speed and feed rate should be properly determined to maintain machining quality while avoiding excessive tool wear and tool tip breakage. Figure 6 depicts the chip morphology owing to the material's plastic softening behavior during cutting, whereas Figure 7 illustrates the observations referring to tool tip wear. These indications were observed in the 16th experimental run and a new tool tip was used to continue with the rest of the experiments. Finally, Figure 8 depicts indicative microscopic textures of machined surfaces. Emphasis has been given to machined textures with noticeable observations.

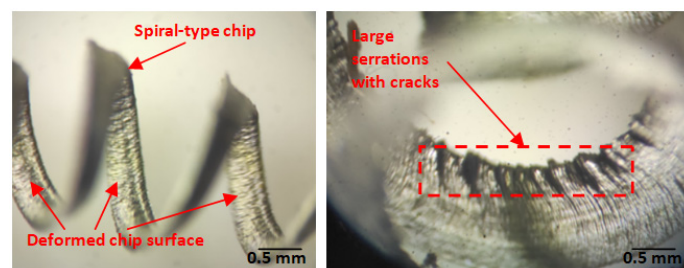


Figure 6. Chip morphology during dry hard-turning of 60CrMoV18-5 cold-work tool steel with CBN cutting insert.

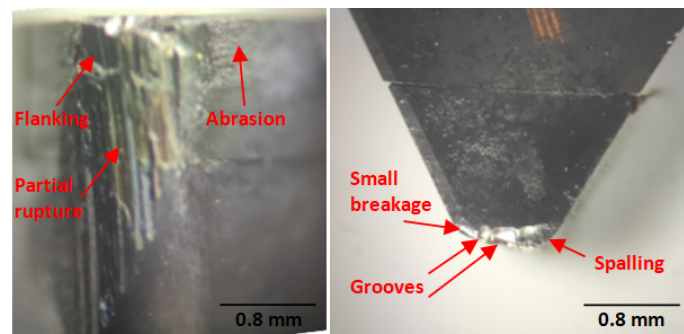


Figure 7. Surface morphology of CBN cutting insert during dry hard-turning of 60CrMoV18-5 cold-work tool steel.

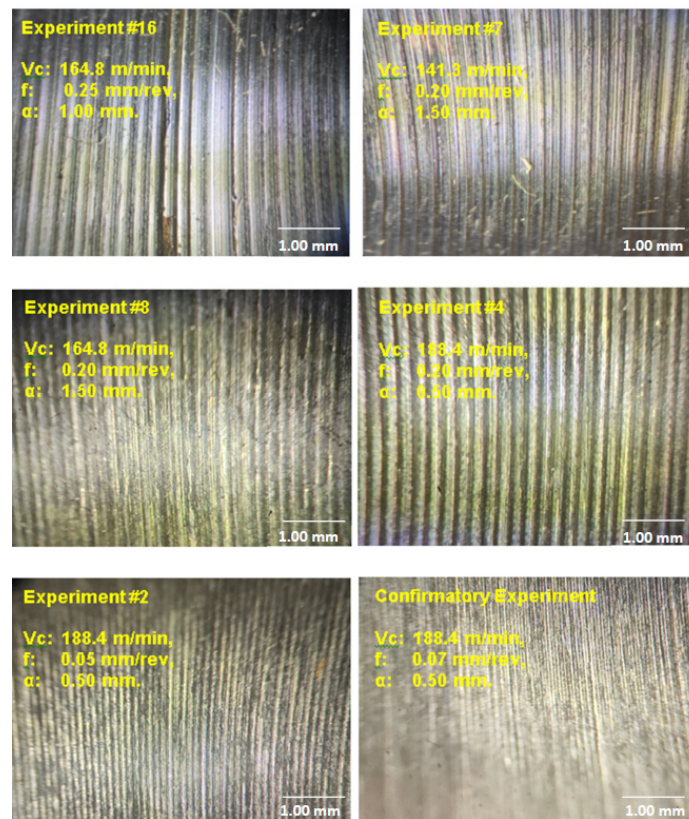


Figure 8. Indicative microscopic textures of machined surfaces during dry hard-turning of 60CrMoV18-5 cold-work tool steel.

As regards surface roughness, its lowest result ($R_a = 0.98 \mu\text{m}$) is reported in the 2nd and 15th experimental runs. These two experiments have different cutting conditions, i.e., the 2nd experiment ran with $V_c = 188.4 \text{ m/min}$ (spindle speed $n = 2000 \text{ rpm}$), $f = 0.05 \text{ mm/rev}$, and $a = 0.5 \text{ mm}$. The 15th experiment ran with cutting speed $V_c = 164.8 \text{ m/min}$, feed rate $f = 0.025 \text{ mm/rev}$, and depth of cut $a = 1 \text{ mm}$. The result of the main cutting force is 83.80 N, which is the lowest from the entire set of experiments. Figure 9 depicts the main effects of cutting parameters on the response of surface roughness. It is clear that feed rate is the dominant parameter in terms of its main effect on surface roughness, with cutting speed to follow. Depth of cut is shown to be less influential, with an insignificant contribution to the response of surface roughness, R_a .

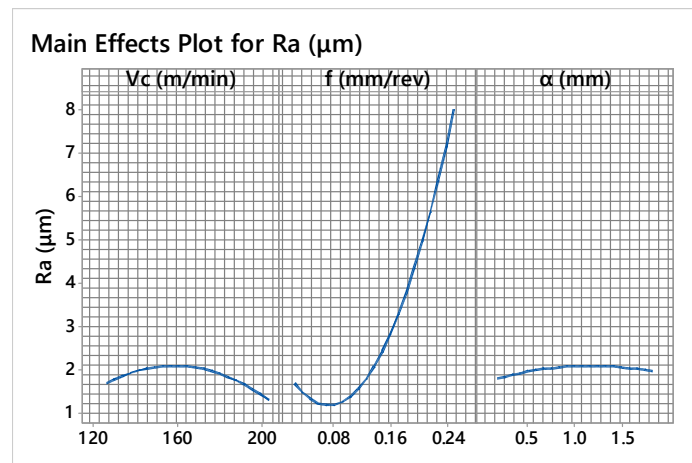


Figure 9. Main effects plot for surface roughness, Ra (μm).

4.2. Analysis of Variance (ANOVA) and Response Surface Regression

To further assess the effect of cutting conditions on machinability indicators of main cutting force F_z (N) and surface roughness Ra (μm), interaction graphs and contour plots were generated. These instances were produced by selecting a regression analysis with full quadratic (second order) models that correlate the independent variables (cutting conditions) with main cutting force F_z and surface roughness Ra . Figure 10 groups the resulting plots concerning the effect of cutting conditions on main cutting force, F_z (N). Figure 10a depicts the interaction effect among the pairs of cutting parameters. It is observed that a strong interaction exists between feed rate f and depth of cut α . Figure 10b corresponds to the effect of cutting speed V_c and feed rate f . It is observed that main cutting force tends to be reduced when operating with low feeds (i.e., 0.05 mm/rev to 0.1 mm/rev) and several cutting speed levels, with emphasis on a range between 160 and 170 m/min for the working material and the cutting tool used. Figure 10c corresponds to the synergistic effect of cutting speed V_c and depth of cut α . Based on the indicative regions of the graph, it can be seen that main cutting force F_z is maintained to low magnitudes for the entire operational range of cutting speed V_c , with a noticeable benefit when setting from 150 m/min to approximately 175 m/min. This assumption imposes the usage of low depth of cut, i.e., from 0.2 mm to approximately 0.5 mm. Figure 10d depicts the synergistic effect between feed rate f (mm/rev) and depth of cut α (mm). The general outcome is that reduced magnitudes of main cutting force F_z are obtained for relatively low feeds and depths, with emphasis to moderate feeds in a range from 0.1 mm/rev to 0.16 mm/rev.

Similarly to the objective of main cutting force F_z , surface roughness Ra was also examined in terms of the effect of cutting conditions and the beneficial response surface regions indicated by the analogous plots. Figure 11 illustrates this group of results. Figure 11a depicts the interaction effect among the pairs of cutting parameters. It is observed that noticeable interactions are found between cutting speed V_c and depth of cut, α as well as feed rate f and depth of cut, α . Figure 11b shows the effect of cutting speed V_c and feed rate f . The contour plot indicates that beneficial results for low surface roughness may be obtained by setting a low feed rate (i.e., 0.05 mm/rev to 0.15 mm/rev) while selecting any value for cutting speed, referring to the experimental range between 130 and 200 m/min. Figure 11c shows that the entire domain referring to the synergistic effect of cutting speed and depth of cut is advantageous for surface roughness, with emphasis on moderate settings for both cutting parameters, i.e., cutting speed $V_c = 155$ m/min to 180 m/min and depth of cut $\alpha = 0.6$ mm to 1.4 mm. Finally, Figure 11d illustrates the contour referring to the synergistic effect between feed rate f and depth of cut α . This contour implies that surface roughness Ra may be maintained to low values concerning feed rate settings, i.e., 0.05 to 0.15 mm/rev, but with obvious fluctuations that tend to increase surface roughness when operating with a depth of cut α from 0.4 to 0.8 mm and from 1.2 to, approximately, 1.75 mm.

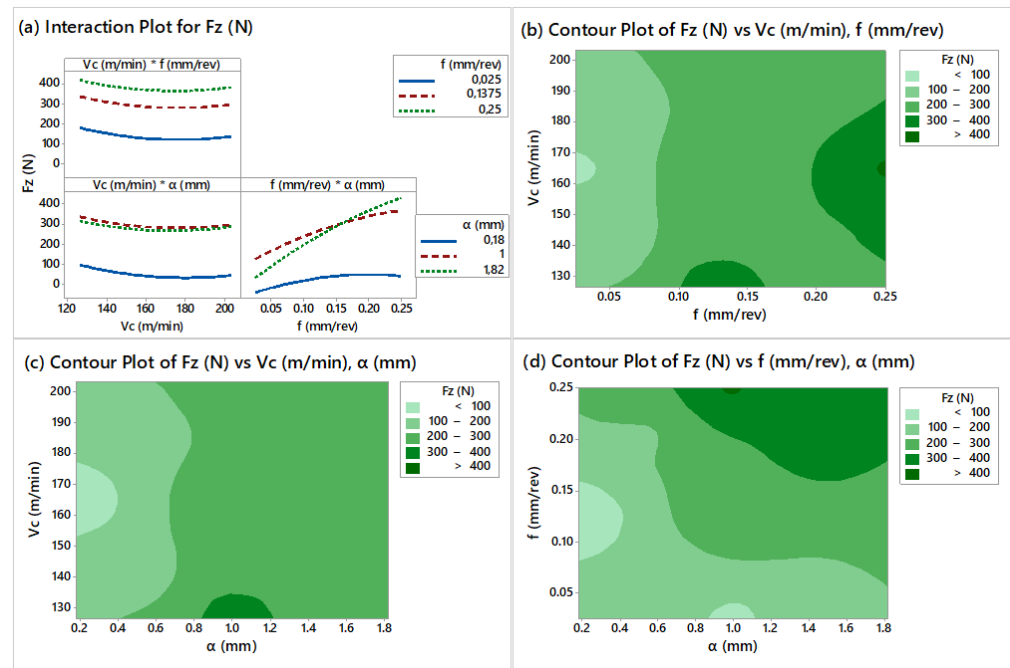


Figure 10. Response contour plots for F_z : (a) Interaction plot for main cutting force F_z ; (b) Contour plot for main cutting force F_z vs. cutting speed V_c and feed rate f ; (c) Contour plot for main cutting force F_z vs. cutting speed V_c and feed rate f ; (d) Contour plot for main cutting force F_z vs. feed rate f and depth of cut α .

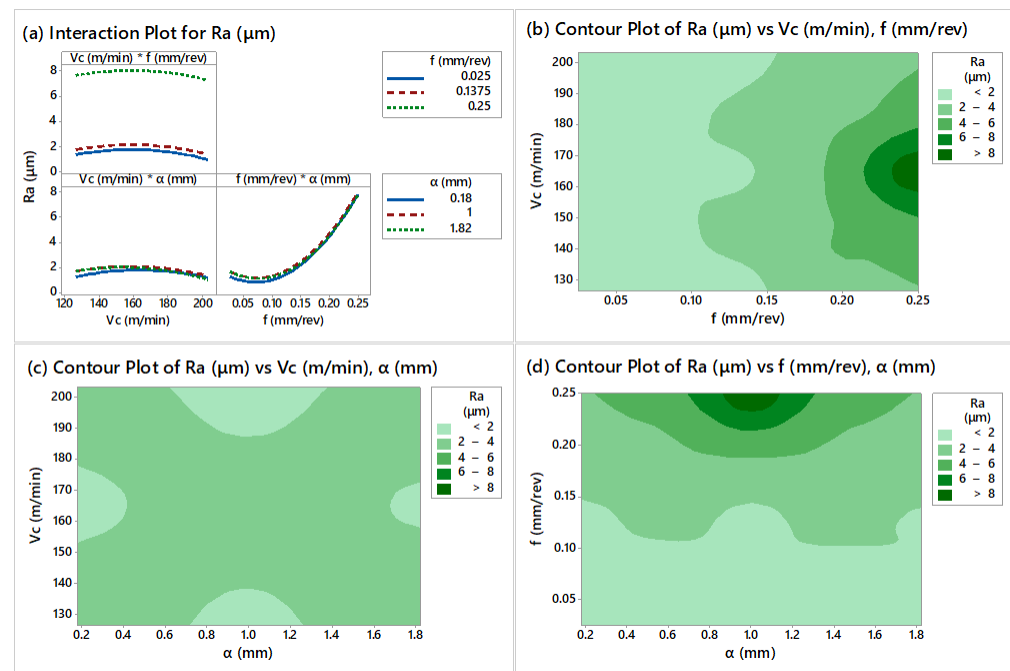


Figure 11. Response contour plots for R_a : (a) Interaction plot for surface roughness R_a ; (b) Contour plot for surface roughness R_a vs. cutting speed V_c and feed rate f ; (c) Contour plot for surface roughness R_a vs. cutting speed V_c and feed rate f ; (d) Contour plot for surface roughness R_a vs. feed rate f and depth of cut α .

Analysis of variance (ANOVA) was conducted on the experimental results so as to estimate the related error and assess the importance of cutting conditions with quantified results. The full quadratic models referring to the machinability objectives of main cutting

force Fz and surface roughness Ra are given in Equation (1) and Equation (2), respectively, as follows:

$$Fz(N) = 612 - 8.29 \times V_c + 933 \times f + 378 \times \alpha + 0.0228 \times V_c^2 - 2899 \times f^2 - 194.1 \times \alpha^2 + 0.48 \times V_c \times f + 0.20 \times V_c \times \alpha + 857 \times f \times \alpha \tag{1}$$

$$Ra(\mu m) = -8.82 + 0.1292 \times V_c - 31.1 \times f + 1.64 \times \alpha - 0.000393 \times V_c^2 + 218.9 \times f^2 - 0.303 \times \alpha^2 + 0.001 \times V_c \times f - 0.0047 \times V_c \times \alpha - 1.20 \times f \times \alpha \tag{2}$$

Tables 3 and 4 tabulate the analysis of variance (ANOVA) results. A p -value lower than 0.05 suggests a term’s significance. p -value for lack-of-fit has to be way beyond from 0.05 to present insignificance. Insignificant lack-of-fit is preferred to support the idea that the model’s error contribution is insignificant and therefore negligible. Both ANOVA tables (Tables 3 and 4) report insignificant lack-of-fit; 0.793 and 0.220, respectively, concerning p -value significance. An adequate correlation coefficient (R^2) for both models is also observed.

Table 3. ANOVA table for response surface regression: Fz (N) vs. V_c, f, a .

| Source | DF | Seq.SS | Contribution % | Adj.SS | Adj.MS | F-Val. | p -Val. |
|----------------|----|---------|----------------|---------|--------|--------|-----------|
| Model | 9 | 192.360 | 90.99 | 192.360 | 21.373 | 11.22 | <0.005 |
| Linear | 3 | 146.571 | 69.33 | 143.425 | 47.808 | 25.09 | <0.005 |
| V_c (m/min) | 1 | 1977 | 0.94 | 1845.0 | 1844.9 | 0.97 | 0.348 |
| f (mm/rev) | 1 | 88.083 | 41.66 | 78.308 | 78.308 | 41.10 | <0.005 |
| a (mm) | 1 | 56.511 | 26.73 | 63.268 | 63.268 | 33.21 | <0.005 |
| Square | 3 | 37.482 | 17.73 | 37.482 | 12.494 | 6.56 | 0.010 |
| V_c^2 | 1 | 3580 | 1.69 | 2114 | 2114.2 | 1.11 | 0.317 |
| f^2 | 1 | 2215 | 1.07 | 2830 | 2829.8 | 1.49 | 0.251 |
| a^2 | 1 | 31.647 | 14.94 | 31.647 | 31.647 | 16.61 | 0.002 |
| 2-way int. | 3 | 8307 | 3.93 | 8307 | 2769 | 1.45 | 0.285 |
| $V_c \times f$ | 1 | 6 | 0.00 | 6 | 5.8 | 0.00 | 0.957 |
| $V_c \times a$ | 1 | 45 | 0.02 | 45 | 45.1 | 0.02 | 0.881 |
| $f \times a$ | 1 | 8256 | 3.91 | 8256 | 8256.1 | 4.33 | 0.064 |
| Error | 10 | 19.051 | 9.01 | 19.051 | 1905.1 | | |
| Lack-of-fit | 5 | 6002 | 2.84 | 6002 | 1200.3 | 0.46 | 0.793 |
| Pure error | 5 | 13.050 | 6.17 | 13.050 | 2609.9 | | |
| Total | 19 | 211.412 | 100 | | | | |
| R^2 | | 90.99% | | | | | |

Table 4. ANOVA table for response surface regression: Ra (μm) vs. V_c, f, a .

| Source | DF | Seq.SS | Contribution % | Adj.SS | Adj.MS | F-Val. | p -Val. |
|----------------|----|---------|----------------|---------|---------|--------|-----------|
| Model | 9 | 62.7894 | 95.43 | 62.7894 | 6.9766 | 23.19 | <0.005 |
| Linear | 3 | 45.6637 | 69.40 | 54.0243 | 18.0081 | 59.85 | <0.005 |
| V_c (m/min) | 1 | 0.1783 | 0.27 | 0.1693 | 0.1693 | 0.56 | 0.470 |
| f (mm/rev) | 1 | 45.4405 | 69.06 | 53.8218 | 53.8218 | 178.88 | <0.005 |
| a (mm) | 1 | 0.0449 | 0.07 | 0.0325 | 0.0325 | 0.11 | 0.749 |
| Square | 3 | 17.0853 | 25.97 | 17.0853 | 5.6951 | 18.93 | <0.005 |
| V_c^2 | 1 | 0.7883 | 1.20 | 0.6288 | 0.6288 | 2.09 | 0.179 |
| f^2 | 1 | 16.2201 | 24.65 | 16.1315 | 16.1315 | 53.61 | <0.005 |
| a^2 | 1 | 0.0768 | 0.12 | 0.0768 | 0.0768 | 0.26 | 0.624 |
| 2-way int. | 3 | 0.0404 | 0.06 | 0.0404 | 0.0135 | 0.04 | 0.987 |
| $V_c \times f$ | 1 | 0.0000 | 0.00 | 0.0000 | 0.0000 | 0.00 | 0.990 |
| $V_c \times a$ | 1 | 0.0242 | 0.04 | 0.0242 | 0.0242 | 0.08 | 0.783 |
| $f \times a$ | 1 | 0.0162 | 0.02 | 0.0162 | 0.0162 | 0.05 | 0.821 |
| Error | 10 | 3.0088 | 4.57 | 3.0088 | 0.3009 | | |
| Lack-of-fit | 5 | 2.6696 | 4.06 | 2.6696 | 0.5339 | 7.87 | 0.220 |
| Pure error | 5 | 0.3393 | 0.52 | 0.3393 | 0.0679 | | |
| Total | 19 | 65.7983 | 100 | | | | |
| R^2 | | 95.43% | | | | | |

An additional statistical analysis to examine the validity of regression models in terms of their correlation capability is the “Anderson–Darling” normality test for residuals. This further validates the strength of the models. In this statistical test, the residuals should follow a normal distribution and exhibit an insignificant contribution to the statistical test by obtaining a p -value result beyond the pre-set confidence interval (C.I.), which is 0.05 or 95%. Both predictive models have been shown to be reliable based on their R^2 coefficients and the p -values for their residuals. Figure 12 illustrates the normal distribution of the residuals of both models: main cutting force F_z (Figure 12a) and surface roughness R_a (Figure 12b). The resulting p -values are 0.224 and 0.235 beyond the confidence interval of 0.05 (95%).

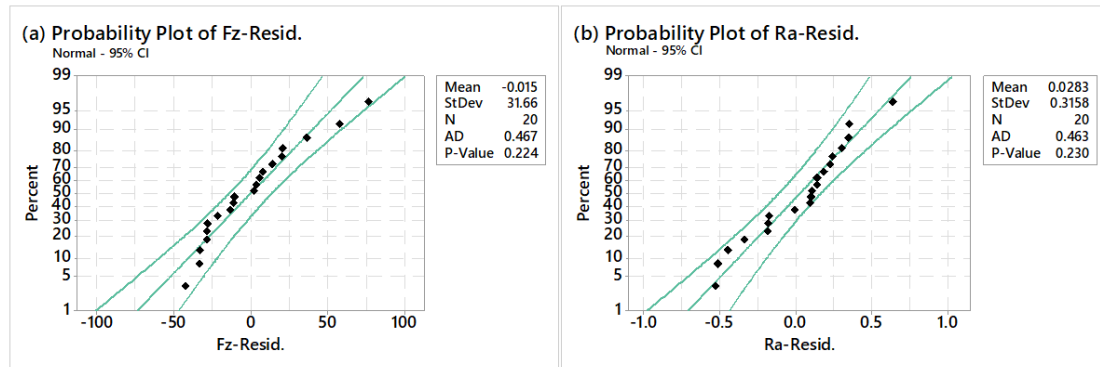


Figure 12. Probability plots for residuals of regression models: (a) main cutting force F_z ; (b) surface roughness R_a .

4.3. Optimization Problem Definition and Solving Using the NSGA-III

The optimization problem was established according to Equations (1) and (2), with reference to the design of experiments and the regression analysis conducted on the experimental and statistical results presented. The design of the experiments, as well as the analysis of results including statistics, was conducted using Minitab® 17 statistical computing environment. The regression models play the role of objective functions of the two-objective optimization problem, whereas the experimental ranges of cutting conditions constitute the constrained search domain for the NSGA-III algorithm’s operators towards the identification of non-dominated optimal solutions. Equations (3) and (4) represent the objective functions, one per machinability criterion for main cutting force F_z (N) and surface roughness R_a (μm), expressed as follows:

$$\min F_z(\text{N}) = 612 - 8.29 \times V_c + 933 \times f + 378 \times \alpha + 0.0228 \times V_c^2 - 2899 \times f^2 - 194.1 \times \alpha^2 + 0.48 \times V_c \times f + 0.20 \times V_c \times \alpha + 857 \times f \times \alpha \quad (3)$$

$$\min R_a(\mu\text{m}) = -8.82 + 0.1292 \times V_c - 31.1 \times f + 1.64 \times \alpha - 0.000393 \times V_c^2 + 218.9 \times f^2 - 0.303 \times \alpha^2 + 0.001 \times V_c \times f - 0.0047 \times V_c \times \alpha - 1.20 \times f \times \alpha \quad (4)$$

These two relations between cutting conditions and machinability criteria (independent variables-inputs and dependent targets-outputs) are subjected to the following constraints:

$$\begin{aligned} V_c \text{ (m/min): } & 141.3 \leq V_c \leq 188.4 \\ f \text{ (mm/rev): } & 0.05 \leq f \leq 0.2 \\ \alpha \text{ (mm): } & 0.5 \leq \alpha \leq 1.5 \end{aligned}$$

The NSGA-III operational parameters were set with reference to the recommended values, whereas the number of individuals (or search agents) was set to 20 [37,38]. The number of iterations for the NSGA-III algorithm was set equal to 1000. The number of non-dominated solutions in the storage archive was set to 50 to simultaneously ensure the quality of solutions by this relatively large solutions number, but with the smallest negative impact as regards the update speed of solutions during the evaluated generations by the algorithm. Algorithmic evaluation experiments were conducted in Mathworks® MATLAB R2013a using a DELL® computer equipped with an Intel® core™ i3–4160 CPU,

3.60 GHz, 64-bit operating system with 12 GB RAM. Figure 13 depicts the Pareto front of non-dominated solutions obtained by NSGA-III algorithm.

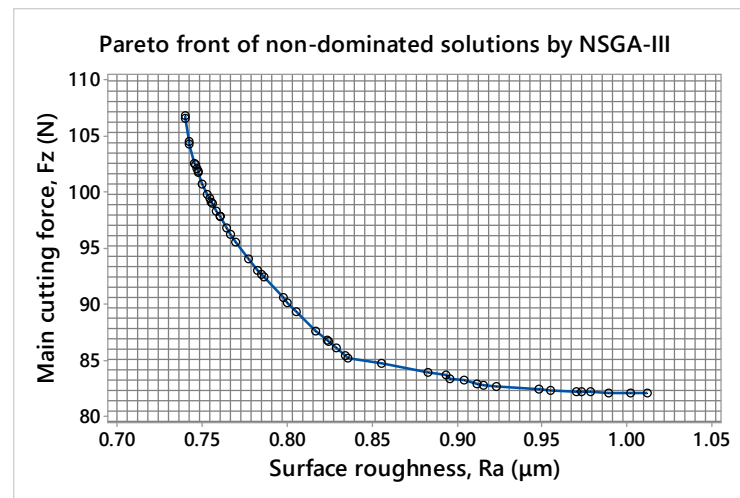


Figure 13. Non-dominated solutions obtained by NSGA-III algorithm.

By observing the Pareto front of non-dominated solutions obtained by NSGA-III, a uniform distribution among the solution points is indicated. This implies that different requirements in terms of main cutting force F_z and surface roughness R_a may be met, provided that the solution range will be constrained to the experimental limits set for this study. In a multi-objective optimization problem, the solutions are characterized as non-dominated when improvement for a criterion is achieved at the expense of at least one other optimization criterion. This implies that no solution may fully optimize all objectives simultaneously. Most advantageous solutions may be found close to the Pareto front's axes origin for criteria minimization requirements. In addition, coverage and spacing are two essential observations that characterize the quality of solutions existing in the multi-objective space and depicted through the Pareto front. Coverage expresses the adequacy of covering all regions of the objective domain with solutions, whereas spread indicates the distance between these solutions.

A quite uniform spread of solutions is observed, satisfying both objectives. Several of the obtained solutions cover the center of the Pareto front, sitting closer to the origin for both axes, thus minimizing simultaneously main cutting force F_z and surface roughness R_a to the best possible extent. The lowest result for main cutting force F_z is reported in the 34th solution, where main cutting force is equal to 82.13 N with cutting parameter values $V_c = 178.8$ m/min, $f = 0.05$ mm/rev, and depth of cut $a = 0.5$ mm. At the same time, the resulting surface roughness R_a is equal to 1.01 μm . Seeking the lowest result for surface roughness, the 26th solution reports 0.74 μm with main cutting force F_z to be equal to 104.3 N. This solution comes with cutting speed $V_c = 188.4$ m/min, feed rate $f = 0.07$, and depth of cut $a = 0.5$ mm.

4.4. Confirmatory CNC Dry Hard-Turning Experiment

To confirm the results obtained by the NSGA-III algorithm, the 26th non-dominated solution's results for cutting parameters in terms of surface roughness were applied to compare the outputs. The position of the cutting insert was such that a new tool tip was used for executing the confirmation experiment. The confirmatory cut along with its corresponding roughness measurement was performed to a cylindrical region close to the work-holding fixture (lathe chuck) to avoid imminent vibrations that could jeopardize the results. The cutting conditions for performing the experiment were $V_c = 188.4$ m/min, $f = 0.07$ mm/rev, and depth of cut $a = 0.5$ mm. The resulting surface roughness R_a was found equal to 0.529 μm . Figure 14 illustrates the roughness measurement environment for

the confirmatory experiment by applying the recommended values for cutting conditions obtained by NSGA-III.

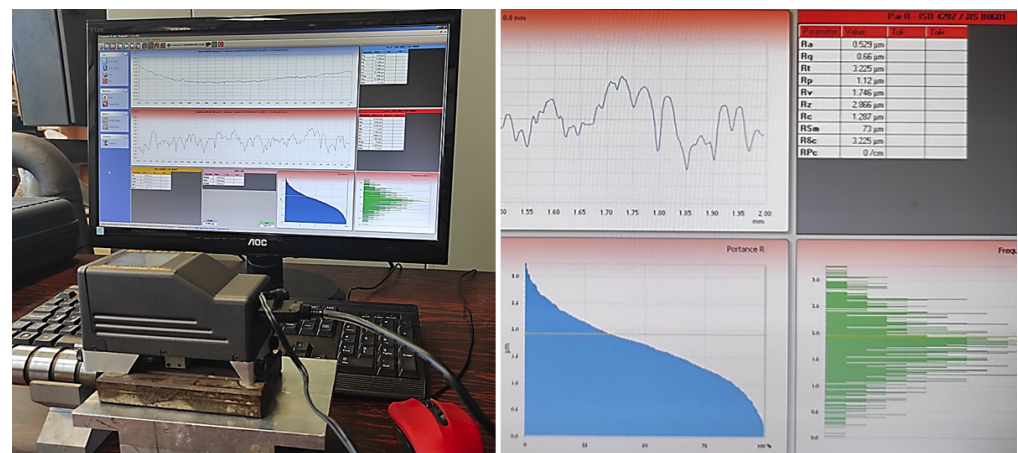


Figure 14. Surface roughness confirmatory experiment using a selected NSGA–III solution.

As regards cutting force magnitude during hard turning, no extreme indications related to cutting tool wear and breakage were observed, except from the 16th experimental run, where flank wear, abrasion, and small tool breakage-grooving were experienced. Therefore, to avoid time-consuming set-ups for establishing the cutting force measuring system along with its peripherals, the confirmatory experiment assessed only surface finish.

To compare the experimental results with those obtained by NSGA-III for surface roughness, an interval plot was generated by considering the two independent samples of surface roughness results and their standard deviations. According to Figure 15, the means of the two sets are different since no overlapping is indicated. It can be observed that the values related to surface roughness are significantly lower than those obtained in actual cutting experiments. In addition, the width of the plot related to the algorithm's obtained results for surface roughness R_a is lower than that corresponding to the experimental results. This observation indicates lower variation in predicted values compared to experiments for surface roughness, whilst no overlapping is found, meaning that the two groups are significantly different at the confidence level.

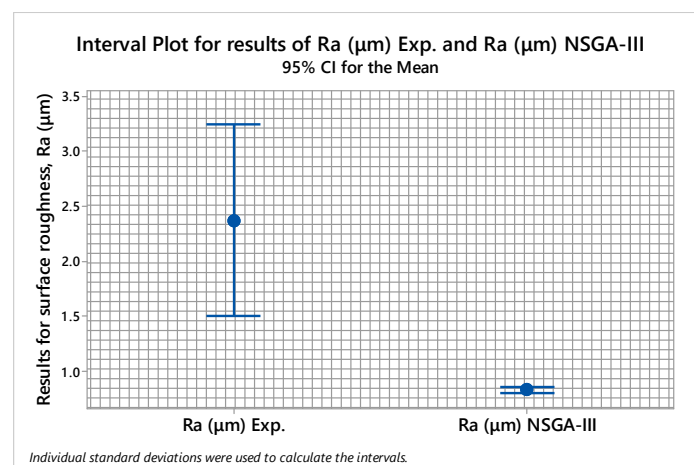


Figure 15. Interval plot for comparing experimental results for surface roughness with the results obtained by NSGA–III.

5. Conclusions

This study examined the machinability of 60CrMoV18-5 cold-work tool steel by conducting a central composite experimental design (CCD) with 20 runs. Machining was conducted using a CNC machine tool for hard dry-turning cuts and a CBN cutting insert (the SECO®, TNGA332S-00820-L1-C). ANOVA and full quadratic regression analysis were applied for the statistical analysis of the experimental results, referring to main cutting force F_z and surface roughness R_a . Machinability observations were reported and the effect of cutting conditions was presented using contour plots by questioning a pair of two independent variables on a performance machinability criterion. By generating two full quadratic regression relations adhering to response surface methodology, the non-dominated sorting genetic algorithm NSGA-III was applied for solving the trade-off between minimum main cutting force F_z and minimum surface roughness R_a . The validity of using the regression models as objective functions for algorithmic evaluations was tested through the correlation coefficient (R^2) and normal probability plots of the residuals corresponding to the two machinability indicators selected: main cutting force F_z and surface roughness R_a . The findings of this study are summarized as follows:

- The interaction between cutting tool and work piece should be carefully examined owing to phenomena related to material softening. Cutting conditions with emphasis on dry hard turning should be carefully selected to sustain low cutting force magnitudes and fine surface finish.
- All cutting force components, -with emphasis on main cutting force, F_z , increase by increasing feed rate and depth of cut. Cutting temperature and resultant material softening may gradually reduce cutting force with noticeable reduction in surface finish.
- Surface roughness is primarily affected by feed rate followed by cutting speed, whereas depth of cut does not yield a strong effect. This result is quite encouraging, since high material removal rates and minimized machining times by applying relatively high cutting depths may be obtained. However, this should be further examined to guarantee the maximum advantageous limit for machining time reduction and high surface finish.
- The NSGA-III algorithm obtained advantageous non-dominated solutions for process planners to select from, given the production needs and constraints. Both machinability criteria, main cutting force F_z and surface roughness R_a , exhibited a quite complex experimental search domain. This observation can justify the implementation of intelligent algorithms to solve multi-criteria machining optimization problems.
- The results obtained agree with notable research findings available in the broader literature concerning the machinability of special engineering alloys, whilst the statistical analysis confirmed initially established research assumptions and expectations referring to main cutting force F_z and surface roughness R_a attributes as key machinability criteria.
- The major objectives of interest are surface integrity and surface finish. Therefore, based on the results obtained, the lowest experimental output for surface roughness R_a is equal to 0.98 μm while the non-dominated solution obtained by NSGA-III algorithm and applied for confirmation experiment was found equal to 0.74 μm . The gain between these two results is 24.49%, whilst by implementing the NSGA-III recommended values for cutting conditions the resultant surface roughness R_a was found equal to 0.53 μm . By comparing the actual confirmatory run to the lowest experimental run from the design of experiments established, a gain is observed equal to 45.92% in terms of surface finish.

In our future perspectives, the authors plan to conduct additional machining experiments to other engineering metals and alloys and different cutting tools. We also plan to implement different intelligent and machine learning modules for optimizing and improving conventional/non-conventional material removal processes. Of major interest for future work is the establishment of optimization problems related to industrial production

and manufacturing systems for boosting productivity, reducing idle times, and increasing surface quality.

Author Contributions: Conceptualization, N.A.F. and N.M.V.; methodology, N.A.F. and N.M.V.; software, N.A.F. and I.G.P.; validation, N.A.F. and I.G.P.; formal analysis, N.A.F. and I.G.P.; investigation, N.A.F. and I.G.P.; resources, N.M.V. and D.E.M.; data curation, N.A.F., I.G.P. and N.M.V.; writing—original draft preparation, N.A.F.; writing—review and editing, N.A.F., I.G.P. and N.M.V.; visualization, N.M.V.; supervision, N.M.V. and D.E.M.; project administration, D.E.M. and N.M.V. All authors have read and agreed to the published version of the manuscript.

Funding: This research received no external funding.

Institutional Review Board Statement: Not applicable.

Informed Consent Statement: Not applicable.

Data Availability Statement: Data are contained within the article.

Conflicts of Interest: The authors declare no conflicts of interest.

References

- Isik, Y. Investigating the machinability of tool steels in turning operation. *Mater. Des.* **2007**, *28*, 1417–1424. [\[CrossRef\]](#)
- Balanou, M.; Karmiris-Obratański, P.; Leszczyńska-Madej, B.; Papazoglou, E.L.; Markopoulos, A.P. Investigation of Surface Modification of 60CrMoV18-5 Steel by EDM with Cu-ZrO₂ Powder Metallurgy Green Compact Electrode. *Machines* **2021**, *9*, 268. [\[CrossRef\]](#)
- Kumar, P.; Dewangan, S.; Pandey, C. Analysis of surface integrity and dimensional accuracy in EDM of P91 steels. *Proc. Mater. Today* **2020**, *33*, 5378–5383. [\[CrossRef\]](#)
- Günay, M.; Korkmaz, M.E. Understanding the Relationship between Surface Quality and Chip Morphology under Sustainable Cutting Environments. *Materials* **2024**, *17*, 1826. [\[CrossRef\]](#)
- Biruk-Urban, K.; Zagórski, I.; Kulisz, M.; Lelen, M. Analysis of Vibration, Deflection Angle and Surface Roughness in Water-Jet Cutting of AZ91D Magnesium Alloy and Simulation of Selected Surface Roughness Parameters Using ANN. *Materials* **2023**, *16*, 3384. [\[CrossRef\]](#)
- Mouralova, K.; Benes, L.; Zahradnicek, R.; Bednar, J.; Zadera, A.; Fries, J.; Kana, V. WEDM Used for Machining High Entropy Alloys. *Materials* **2020**, *13*, 4823. [\[CrossRef\]](#)
- Kenda, J.; Pusavec, F.; Kermouche, G.; Kopac, J. Surface Integrity in Abrasive Flow Machining of Hardened Tool Steel AISI D2. *Proc. Eng.* **2011**, *19*, 172–177. [\[CrossRef\]](#)
- Boujelbene, M.; Ezeddini, S.; Ben Said, L.; Bayraktar, E.; Alhadri, M.; Aich, W.; Ghachem, K.; Kolsi, L. Analysis of surface integrity of intermetallic composite based on titanium-aluminum machined by laser cutting. *Opt. Laser Technol.* **2023**, *161*, 109187. [\[CrossRef\]](#)
- Bouacha, K.; Yallese, M.A.; Mabrouki, T.; Rigal, J.-F. Statistical analysis of surface roughness and cutting forces using response surface methodology in hard turning of AISI 52100 bearing steel with CBN tool. *Int. J. Refract. Hard Mater.* **2010**, *28*, 349–361. [\[CrossRef\]](#)
- Patel, V.D.; Gandhi, A.H. Analysis and modeling of surface roughness based on cutting parameters and tool nose radius in turning of AISI D2 steel using CBN tool. *Measurement* **2019**, *138*, 34–38. [\[CrossRef\]](#)
- Lalwani, D.I.; Mehta, N.K.; Jain, P.K. Experimental investigations of cutting parameters influence on cutting forces and surface roughness in finish hard turning of MDN250 steel. *J. Mater. Process. Technol.* **2008**, *206*, 167–179. [\[CrossRef\]](#)
- Sahoo, A.K.; Sahoo, B. Experimental investigations on machinability aspects in finish hard turning of AISI 4340 steel using uncoated and multilayer coated carbide inserts. *Measurement* **2012**, *45*, 2153–2165. [\[CrossRef\]](#)
- Li, X.; Liu, X.; Yue, C.; Liang, S.Y.; Wang, L. Systematic review on tool breakage monitoring techniques in machining operations. *Int. J. Mach. Tools Manuf.* **2022**, *176*, 103882. [\[CrossRef\]](#)
- Benlahmidi, S.; Aouici, H.; Boutaghane, F.; Khellaf, A.; Fnides, B.; Yallese, M.A. Design optimization of cutting parameters when turning hardened AISI H11 steel (50 HRC) with CBN7020 tools. *Int. J. Adv. Manuf. Technol.* **2017**, *89*, 803–820. [\[CrossRef\]](#)
- Çydaş, U. Machinability evaluation in hard turning of AISI 4340 steel with different cutting tools using statistical techniques. *Proc. Inst. Mech. Eng. B J. En. Manuf.* **2010**, *224*, 1043–1055. [\[CrossRef\]](#)
- Santhosh, A.J.; Tura, A.D.; Jiregna, I.T.; Gemechu, W.F.; Ashok, N.; Ponnusamy, M. Optimization of CNC turning parameters using face centred CCD approach in RSM and ANN-genetic algorithm for AISI 4340 alloy steel. *Res. Eng.* **2021**, *11*, 100251. [\[CrossRef\]](#)
- Abbas, A.T.; Al-Abduljabbar, A.A.; Alnaser, I.A.; Aly, M.F.; Abdelgalil, I.H.; Elkaseer, A. A Closer Look at Precision Hard Turning of AISI4340: Multi-Objective Optimization for Simultaneous Low Surface Roughness and High Productivity. *Materials* **2022**, *15*, 2106. [\[CrossRef\]](#)

18. Chavan, A.; Sargade, V. Surface Integrity of AISI 52100 Steel during Hard Turning in Different Near-Dry Environments. *Adv. Mater. Sci. Eng.* **2020**, *2020*, 1–13. [[CrossRef](#)]
19. Davoudinejada, A.; Noordin, M.Y.; Ghodsiyehc, D.; Ashrafi, S.A.; Barzani, M.M. Effect of Tool Wear on Tool Life and Surface Finish when Machining DF-3 Hardened Tool Steel. *Appl. Mech. Mater.* **2013**, *315*, 241–245. [[CrossRef](#)]
20. Sun, F.J.; Qu, S.G.; Pan, Y.X.; Li, X.Q.; Li, F.L. Effects of cutting parameters on dry machining Ti-6Al-4V alloy with ultra-hard tools. *Int. J. Adv. Manuf. Technol.* **2015**, *79*, 351–360. [[CrossRef](#)]
21. Muthuswamy, P.; Murugesan, V.G.V. Machinability analysis in high speed turning of Ti-6Al-4V alloy and investigation of wear mechanism in AlTiN PVD coated tungsten carbide tool. *Eng. Res. Express* **2021**, *3*, 045011. [[CrossRef](#)]
22. Malik, A.; Singh, A.K.; Prakash, A.; Mali, H.S. Experimental analysis for turning of Ti6Al4V alloy by tungsten carbide coated tool inserts. *Mater. Today Proc.* **2023**, *92*, 11–16. [[CrossRef](#)]
23. Li, G.; Xu, W.; Jin, X.; Liu, L.; Ding, S.; Li, C. The machinability of stainless steel 316 L fabricated by selective laser melting: Typical cutting responses, white layer and evolution of chip morphology. *J. Mater. Process. Technol.* **2023**, *315*, 117926. [[CrossRef](#)]
24. Rathod, N.J.; Chopra, M.K.; Chaurasiya, P.K.; Pawar, S.H.; Tiwari, D.; Kumar, R.; Saxena, K.K.; Buddhi, D. Design and optimization of process parameters for hard turning of AISI 304 stainless steel using Taguchi-GRA-PCA. *Int. J. Interact. Des. Manuf.* **2023**, *17*, 2403–2414. [[CrossRef](#)]
25. Binali, R.; Demirpolat, H.; Kuntoglu, M.; Salur, E. Different Aspects of Machinability in Turning of AISI 304 Stainless Steel: A Sustainable Approach with MQL Technology. *Metals* **2023**, *13*, 1088. [[CrossRef](#)]
26. Khan, M.M.A.; Mithu, M.A.H.; Dhar, N.R. Effects of minimum quantity lubrication on turning AISI 9310 alloy steel using vegetable oil-based cutting fluid. *J. Mater. Process. Technol.* **2009**, *209*, 5573–5583. [[CrossRef](#)]
27. Moganapriya, C.; Rajasekar, R.; Santhosh, R.; Saran, S.; Santhosh, S.; Gobinath, V.K.; Kumar, P.S. Sustainable Hard Machining of AISI 304 Stainless Steel Through TiAlN, AlTiN, and TiAlSiN Coating and Multi-Criteria Decision Making Using Grey Fuzzy Coupled Taguchi Method. *J. Mater. Eng. Perform.* **2022**, *16*, 7302–7314. [[CrossRef](#)]
28. Dhilip, J.D.J.; Jeevan, J.; Arulkirubakaran, D.; Ramesh, M. Investigation and optimization of parameters for hard turning of OHNS steel. *Mater. Manuf. Process.* **2020**, *35*, 1113–1119. [[CrossRef](#)]
29. Sangwan, K.S.; Saxena, S.; Kant, G. Optimization of Machining Parameters to Minimize Surface Roughness using Integrated ANN-GA Approach. *Proc. CIRP* **2015**, *29*, 305–310. [[CrossRef](#)]
30. Sivarajan, S.; Elango, M.; Sasikumar, M.; Doss, A.S.A. Prediction of surface roughness in hard machining of EN31 steel with TiAlN coated cutting tool using fuzzy logic. *Mater. Today Proc.* **2022**, *65*, 35–41. [[CrossRef](#)]
31. Vasanth, X.A.; Paul, P.S.; Varadarajan, A.S. A neural network model to predict surface roughness during turning of hardened SS410 steel. *Int. J. Syst. Assur. Eng. Manag.* **2020**, *11*, 704–715. [[CrossRef](#)]
32. Das, P.P.; Chakraborty, S. SWARA-CoCoSo method-based parametric optimization of green dry milling processes. *J. Eng. Appl. Sci.* **2022**, *69*, 1–21. [[CrossRef](#)]
33. Ghosh, T.; Martinsen, K. NSGA III for CNC End Milling Process Optimization. In *Machine Learning and Metaheuristics Algorithms, and Applications*; Thampi, S., Trajkovic, L., Li, K.C., Das, S., Wozniak, M., Berretti, S., Eds.; SoMMA 2019. Communications in Computer and Information Science; Springer: Singapore, 2020; Volume 1203. [[CrossRef](#)]
34. Gajević, S.; Marković, A.; Milojević, S.; Ašonja, A.; Ivanović, L.; Stojanović, B. Multi-objective optimization of tribological characteristics for aluminum composite using taguchi grey and TOPSIS approaches. *Lubricants* **2024**, *12*, 171. [[CrossRef](#)]
35. Bukvić, M.; Gajević, S.; Skulić, A.; Savić, S.; Ašonja, A.; Stojanović, B. Tribological Application of Nanocomposite Additives in Industrial Oils. *Lubricants* **2024**, *12*, 6. [[CrossRef](#)]
36. Myers, R.H.; Montgomery, D.C. *Response Surface Methodology—Process and Product Optimization Using Designed Experiments*, 2nd ed.; Wiley Series in Probability and Statistics; Wiley: New York, NY, USA, 2002.
37. Deb, K.; Jain, H. An Evolutionary Many-Objective Optimization Algorithm Using Reference-Point-Based Nondominated Sorting Approach, Part I: Solving Problems With Box Constraints. *IEEE Trans. Evolut. Comput.* **2014**, *18*, 577–601. [[CrossRef](#)]
38. Jain, H.; Deb, K. An Evolutionary Many-Objective Optimization Algorithm Using Reference-Point Based Nondominated Sorting Approach, Part II: Handling Constraints and Extending to an Adaptive Approach. *IEEE Trans. Evolut. Comput.* **2014**, *18*, 602–622. [[CrossRef](#)]

Disclaimer/Publisher’s Note: The statements, opinions and data contained in all publications are solely those of the individual author(s) and contributor(s) and not of MDPI and/or the editor(s). MDPI and/or the editor(s) disclaim responsibility for any injury to people or property resulting from any ideas, methods, instructions or products referred to in the content.